Letter

# Digitally Programmable Resonant Elastic Metamaterials

Christopher Sugino,[1,*] Massimo Ruzzene,[2] and Alper Erturk[1]

[1] *G. W. Woodruff School of Mechanical Engineering, Georgia Institute of Technology, Atlanta, Georgia 30309, USA*

[2] *Department of Mechanical Engineering, University of Colorado Boulder, Boulder, Colorado 80309, USA*

(Received 7 January 2020; revised manuscript received 3 April 2020; accepted 28 April 2020; published 5 June 2020)

We introduce and experimentally demonstrate a class of fully programmable digitally controlled metamaterials. An elastic waveguide is connected to synthetic impedance circuits as active elements to enable simultaneous control over the center frequency, attenuation, and bandwidth of resonant band gaps. The experimental results demonstrate digital tuning over a wide frequency range that spans several modes of the waveguide. This platform opens avenues to achieving precise control over effective metamaterial properties and their possible space-time modulation, paving the way for digitally controlled programmable wave devices.

DOI: 10.1103/PhysRevApplied.13.061001

Elastic metamaterials are engineered materials the architecture of which yields effective properties not found in nature, which generally lead to numerous desirable dynamic properties. These include wave-propagation and vibration-attenuation characteristics that far outperform conventional vibration- and noise-control solutions. Several concepts rely on the occurrence of internal resonances [1] that induce subwavelength band gaps and are suitable for low-frequency vibration attenuation. Other phenomena that have been investigated include negative refraction [2–4], cloaking [5–7], and topologically protected edge states [8,9] in both acoustic and elastic domains. Numerous designs for locally resonant metamaterials have been considered in the literature, leveraging both mechanical [1,10–16] and electromechanical [17–22] local resonators. The attenuation performance of mechanical resonant metamaterials is limited by the added-mass ratio [19], a potentially undesirable trade-off, whereas their electromechanical counterparts are limited by the effective electromechanical coupling [22] achievable by passive shunted circuits. In addition, most existing embodiments of resonant metamaterials lack tunability, as they exhibit a band gap over a fixed frequency range. Thus, to improve the performance and multifunctionality of locally resonant metamaterials, some researchers have investigated techniques to employ semiactive components that induce buckling [23] or use shape-memory alloys [24]. Such solutions are guaranteed to be stable but generally provide limited tunability. Fully active solutions, such as electrical feedback [25,26], have much greater tunability, obtained at the cost of greater power requirements, reduced stability margins, and increased complexity.

Here, we investigate a fully programmable and digitally reconfigurable resonant metamaterial through an electromechanical implementation of an elastic waveguide. The concept employs digital control, which allows the shunt-circuit impedance to be freely varied, so that the resonant band gap can be placed at an arbitrary frequency (details of the theoretical framework can be found in Ref. [27]). While wave attenuation through resonant band gaps is the primary goal of this study, the investigations presented herein serve as an illustration of the level of tunability that can be achieved through the proposed configuration, which may be applied to achieve a number of effective properties and performance characteristics. For example, the use of digital control introduces the possibility for shunt circuits with semiarbitrary linear frequency response and nonlinearity, greatly expanding the design space of metamaterial effective material properties.

We consider a piezoelectric bimorph beam with separately bonded piezoceramics (i.e., piezos), each poled in the thickness direction (Fig. 1). The central shim is electrically grounded and the opposing faces of each patch are covered with thin metallic electrodes. Opposing electrodes are electrically connected (parallel-wire operation) and the resulting electrode pairs are shunted through a synthetic impedance circuit. Each synthetic impedance circuit provides some effective admittance $Y(s) = I(s)/V(s)$, which is normalized by the capacitance of each electrode pair such that $h(s) = Y(s)/C_p$ is the same for each circuit.

Synthetic impedance for piezoelectric shunts was introduced by Fleming *et al.* [28], who described a simple analog circuit that acts as a voltage-controlled current

*csugino3@gatech.edu

 

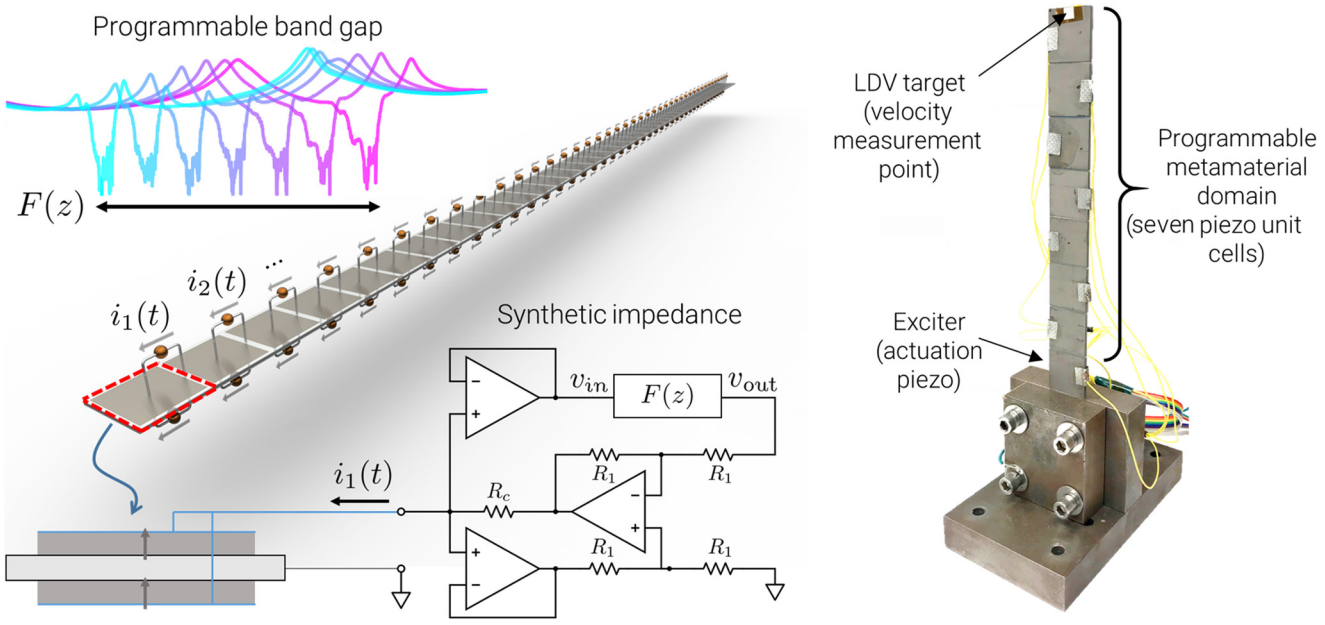


FIG. 1. Left: a schematic of the programmable piezoelectric locally resonant metamaterial with a digitally tunable band gap. Thickness-poled piezoelectric patches are connected in parallel for bending vibration and shunted to synthetic impedance circuits, which have an impedance determined by the digital transfer function $F(z)$. This enables the creation of a fully programmable locally resonant band gap. Right: the experimental realization of the programmable resonant metamaterial.

source, such that the introduction of a digital filter into the loop allows specification of the effective shunt-circuit admittance or impedance. In the present work, the synthetic impedance circuit proposed by Nečásek *et al.* [29], based on the Howland current pump (HCP), is used. This circuit allows one of the terminals to be grounded, making it suitable for an array of separate shunts on the same structure. A diagram of the circuit is provided in Fig. 1.

Assuming the operational amplifiers are ideal, the output current of the circuit in Fig. 1 is

$$i(t) = \frac{v_{\text{out}}(t)}{R_c}. \tag{1}$$

Thus, to establish the desired admittance relationship between the piezoelectric voltage $v_{\text{in}}(t)$ and the supplied current $i(t)$, we introduce a discrete filter $F(z)$ relating the output voltage $v_{\text{out}}(t)$ to the piezoelectric voltage $v_{\text{in}}(t)$, i.e.,

$$V_{\text{out}}(s) = F(s)V_{\text{in}}(s), \tag{2}$$

where $F(s)$ is the effective continuous-time transfer function of the digital filter $F(z)$. The effective admittance of the circuit is then

$$Y(s) = \frac{I(s)}{V_{\text{in}}(s)} = \frac{F(s)}{R_c} \quad \Longrightarrow \quad F(s) = R_c Y(s). \tag{3}$$

For a desired admittance $Y(s)$, the corresponding filter $F(s)$ can be calculated using Eq. (3) and uploaded to the controller. The controller utilizes a field-programmable gate array (FPGA) that is programmed using National Instruments LabVIEW, enabling real-time control of the digital-filter transfer-function coefficients.

The tested system is fabricated from a 2024 aluminum shim and piezoceramic patches made of PZT-5A (Piezo Systems), as shown in Fig. 1. The shim has dimensions 185.9 mm × 22.9 mm × 0.508 mm and each separate piezo has dimensions 22.9 mm × 22.9 mm × 0.508 mm. The piezos are vacuum bonded to the aluminum with epoxy to minimize the bonding-layer thickness, with 0.5 mm between adjacent piezos to reduce the effect of the stiffness mismatch between the bonded and nonbonded areas of the aluminum.

The beam is clamped as a cantilever (i.e., clamped-free) 0.5 mm from the final piezo and the central shim is grounded through the clamping hardware. Measurements are performed by exciting the piezo closest to the clamp with a broadband voltage-noise burst and measuring the velocity at the tip of the beam using a laser Doppler vibrometer (LDV). The resulting frequency response functions (FRFs) between the voltage input and the velocity output are used to characterize the performance of the beam. Parametric sweeps are performed by linearly varying impedance parameters between two set points. For each desired impedance transfer function, the corresponding transfer function $F(s)$ is calculated and uploaded to the controller. The FRF measurements are then carried out with ten averages. This process is automated in a

LabVIEW interface, such that high-resolution parametric sweeps can be performed.

First, experiments are performed to characterize the tunability of the locally resonant band gap of the developed system. A normalized admittance of the form

$$h(s) = \frac{Y(s)}{C_p} = \frac{\omega_t^2}{s} + 2\zeta\omega_t \tag{4}$$

is used, where $C_p$ is the measured piezoelectric capacitance, $\omega_t$ is the resonant frequency of the $LC$ shunt circuit, and $\zeta$ is the damping ratio. Due to phase lag in the system, the actual damping ratio is smaller than indicated by the shunt circuit, with greater deviation at higher frequencies $\omega_t$. Additionally, the bias resistance $R_b$ used to dissipate dc bias current adds additional damping, i.e.,

$$\zeta_b = \frac{1}{2\omega_t R_b C_p}, \tag{5}$$

which becomes smaller for increasing $\omega_t$. For the synthetic shunt circuit used here, $R_b = 1\ \mathrm{M\Omega}$, such that $\zeta_b \approx 1$ occurs at $\omega_t/(2\pi) = 2.5$ Hz. Note that although this additional damping may become significant at low frequencies, there is no restriction on the sign of $\zeta$ in Eq. (4), such that the overall effective damping ratio can be adjusted to be as small as desired. This is illustrated in Fig. 2 for the case $f_t = 78$ Hz and varying $\zeta$. The damping ratio of the synthetic circuit is tunable in a nearly continuous fashion, limited only by the precision of the calculations on the digital controller. It is also worth noting that to achieve an electrical resonance of 78 Hz, the synthetic impedance circuit must provide an equivalent inductance of approximately 135 H, something significantly beyond the capability of analog inductors.

The results for an experimental parameter sweep of $\omega_t/(2\pi)$ between 600 Hz and 1.5 kHz are shown in Fig. 3. The targeted frequency (i.e., the input to the controller) is shown by the dashed line, which closely follows the attenuation region induced by the resonant band gap. This indicates that the developed system exhibits a band gap that can be placed precisely across this full tested frequency range, a significant advancement over previous metamaterial implementations. Furthermore, as highlighted in Fig. 3(b), the locally resonant band gap achieves strong attenuation over its entire bandwidth, unlike a standard antiresonance.

Note that it is necessary to vary the damping ratio $\zeta$ of Eq. (4) along with the target frequency $\omega_t$ to maintain a similar overall damping level in the system while sweeping the locally resonant band gap of Fig. 3: the prescribed damping ratio $\zeta$ is swept linearly from $5.8 \times 10^{-3}$ to $1.68 \times 10^{-2}$ from $\omega_t/(2\pi) = 600$ Hz to 1.5 kHz, respectively. Such parameter adjustment is a unique capability

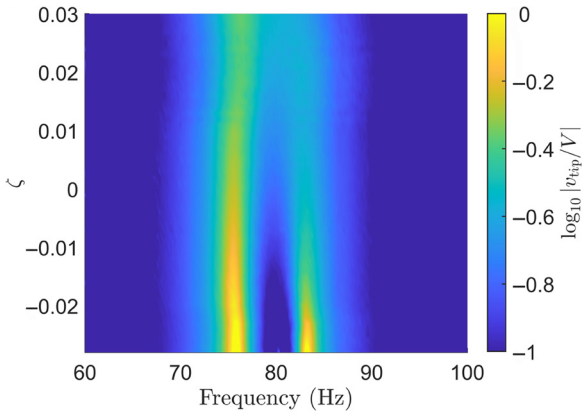


FIG. 2. The experimental tip-velocity FRF for a resonant shunt with $f_t = 78$ Hz and varying damping ratio $\zeta$. Due to freedom of design with synthetic impedance, the damping ratio specified by the circuit can be made negative to cancel the inherent damping present in the structure and circuit. The system becomes unstable near $\zeta = -0.028$.

of the developed system, which is able to tune all shunt-circuit parameters simultaneously. These damping ratios are selected to make the overall damping level small and highlight the attenuation inside the resonant band gap. As a result, there are significant resonant peaks just before and after the band gap [see Fig. 3(b)]. These resonances can be attenuated through the addition of damping [30], as in Fig. 2, although this solution reduces the attenuation inside the resonant band gap. Other potential solutions include the use of higher-order linear shunt circuits (e.g., a compensator [27]) or the introduction of nonlinearity [31]. Such advanced solutions are easily implemented in the synthetic impedance system, but they require careful consideration of the system stability and the power limitations of the circuit.

Next, experiments are performed to investigate a fixed-frequency locally resonant band gap with varying bandwidth. It has been shown that the use of negative capacitance increases the effective electromechanical coupling of the system [19,32], which increases the bandwidth of the locally resonant band gap. To this end, a normalized admittance of the form

$$h(s) = (1-c)\left(\frac{\omega_t^2}{s} + 2\zeta\omega_t\right) - cs \tag{6}$$

is used, where $c$ denotes the fraction of the piezoelectric capacitance being canceled, $\omega_t$ is the targeted shunt resonance, and $\zeta$ is the corresponding damping ratio, included to improve the stability margins. The measured FRFs for $\omega_t/(2\pi) = 780$ Hz and $c = 0$, 0.1, 0.2, and 0.4 are shown in Fig. 4. Note that the band-gap bandwidth can be dramatically increased through the use of

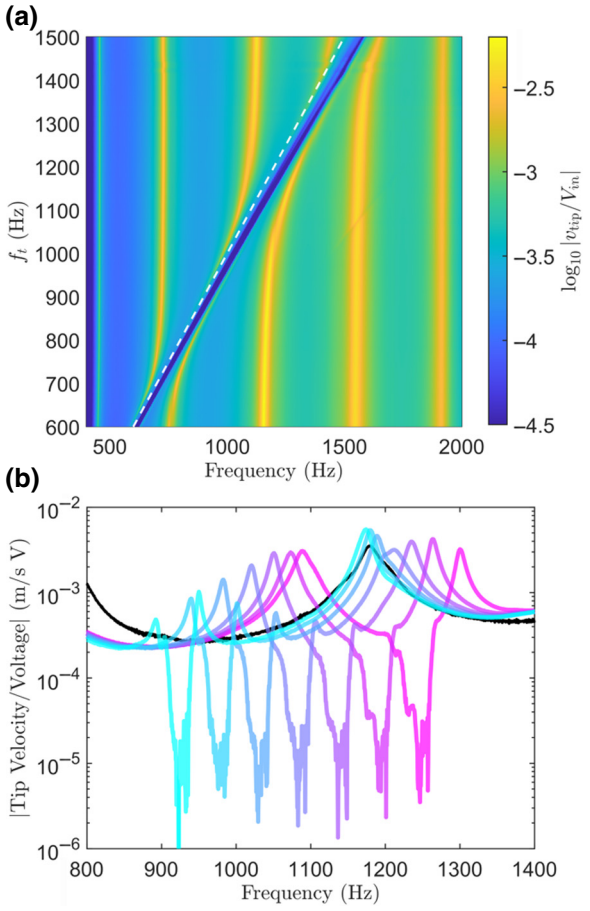


FIG. 3. (a) The experimental tip-velocity FRF versus the frequency and the target frequency $f_t$. The locally resonant band gap and the associated vibration attenuation clearly follow the specified target frequency, shown by the white dashed line. (b) Several highlighted FRFs [horizontal slices from (a)], with $f_t$ ranging from 900 Hz to 1200 Hz in 50-Hz increments. The locally resonant band gap is a distinct flat region of attenuation in each case. The black curve shows the response at open circuit (i.e., with all the circuits disconnected).

negative capacitance and stability can be maintained by a corresponding increase in the damping ratio.

In summary, we experimentally demonstrate an elastic metamaterial the effective material properties of which can be digitally programmed using synthetic impedance shunts. The system exhibits a resonant band gap that can be shifted in a nearly continuous fashion via digital tuning over a wide frequency range, 45 times the bandwidth of a fixed-frequency band gap, spanning a wide range of natural modes. Furthermore, the damping and bandwidth of the band gap can be externally programmed, giving precise control over the dynamic response of the locally resonant metamaterial. Such precise control over effective properties is necessary for the development of active metamaterials, where stability and transient switching effects are of fundamental importance. As such, this

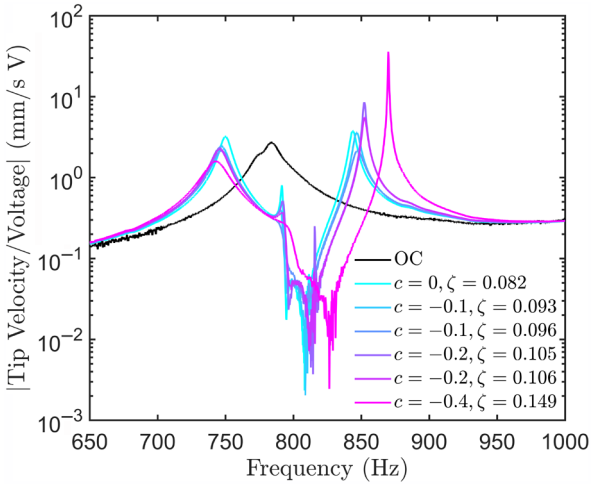


FIG. 4. The measured FRFs for $\omega_t/(2\pi) = 780$ Hz with four different negative capacitance values and various damping ratios. Note that higher damping ratios are required to maintain stability at more negative values of $c$. The open circuit response is shown for reference.

work is a major step toward the realization of metamaterials with prescribed spatial and temporal distributions of effective material properties, facilitating the experimental investigation of wave phenomena such as nonreciprocal wave propagation, topological pumping, and rainbow trapping. Future work will focus on developing systems with larger numbers of programmable unit cells, enabling the measurement of propagating waves and the introduction of gradient properties through spatial variation of circuit parameters.

[1] Z. Liu, X. Zhang, Y. Mao, Y. Y. Zhu, Z. Yang, C. T. Chan, and P. Sheng, Locally resonant sonic materials, Science **289**, 1734 (2000).
[2] L. Fok and X. Zhang, Negative acoustic index metamaterial, Phys. Rev. B **83**, 214304 (2011).
[3] R. Zhu, X. Liu, G. Hu, C.-T. Sun, and G. Huang, Negative refraction of elastic waves at the deep-subwavelength scale in a single-phase metamaterial, Nat. Commun. **5**, 5510 (2014).
[4] S. A. Cummer, J. Christensen, and A. Alù, Controlling sound with acoustic metamaterials, Nat. Rev. Mater. **1**, 16001 (2016).
[5] G. W. Milton, M. Briane, and J. R. Willis, On cloaking for elasticity and physical equations with a transformation invariant form, New J. Phys. **8**, 248 (2006).
[6] S. A. Cummer, B.-I. Popa, D. Schurig, D. R. Smith, J. Pendry, M. Rahm, and A. Starr, Scattering Theory Derivation of a 3D Acoustic Cloaking Shell, Phys. Rev. Lett. **100**, 024301 (2008).
[7] M. Farhat, S. Guenneau, S. Enoch, and A. B. Movchan, Cloaking bending waves propagating in thin elastic plates, Phys. Rev. B **79**, 033102 (2009).

[8] S. H. Mousavi, A. B. Khanikaev, and Z. Wang, Topologically protected elastic waves in phononic metamaterials, Nat. Commun. **6**, 8682 (2015).
[9] Z. Yang, F. Gao, X. Shi, X. Lin, Z. Gao, Y. Chong, and B. Zhang, Topological Acoustics, Phys. Rev. Lett. **114**, 114301 (2015).
[10] K. M. Ho, C. K. Cheng, Z. Yang, X. X. Zhang, and P. Sheng, Broadband locally resonant sonic shields, Appl. Phys. Lett. **83**, 5566 (2003).
[11] H. Peng and P. F. Pai, Acoustic metamaterial plates for elastic wave absorption and structural vibration suppression, Int. J. Mech. Sci. **89**, 350 (2014).
[12] Z. Yang, J. Mei, M. Yang, N. Chan, and P. Sheng, Membrane-Type Acoustic Metamaterial with Negative Dynamic Mass, Phys. Rev. Lett. **101**, 204301 (2008).
[13] H. H. Huang, C. T. Sun, and G. L. Huang, On the negative effective mass density in acoustic metamaterials, Int. J. Eng. Sci. **47**, 610 (2009).
[14] D. Yu, Y. Liu, H. Zhao, G. Wang, and J. Qiu, Flexural vibration band gaps in Euler-Bernoulli beams with locally resonant structures with two degrees of freedom, Phys. Rev. B **73**, 064301 (2006).
[15] Y. Xiao, J. Wen, and X. Wen, Flexural wave band gaps in locally resonant plates with periodically attached spring-mass resonators, J. Phys. D: Appl. Phys. **45**, 195401 (2012).
[16] C. Sugino, Y. Xia, S. Leadenham, M. Ruzzene, and A. Erturk, A general theory for bandgap estimation in locally resonant metastructures, J. Sound Vib. **406**, 104 (2017).
[17] F. Casadei, M. Ruzzene, L. Dozio, and K. A. Cunefare, Broadband vibration control through periodic arrays of resonant shunts: Experimental investigation on plates, Smart Mater. Struct. **19**, 015002 (2009).
[18] Y. Y. Chen, G. L. Huang, and C. T. Sun, Band gap control in an active elastic metamaterial with negative capacitance piezoelectric shunting, J. Vib. Acoust. **136**, 061008 (2014).
[19] C. Sugino, S. Leadenham, M. Ruzzene, and A. Erturk, An investigation of electroelastic bandgap formation in locally resonant piezoelectric metastructures, Smart Mater. Struct. **26**, 055029 (2017).
[20] Y. Chen, G. Hu, and G. Huang, A hybrid elastic metamaterial with negative mass density and tunable bending stiffness, J. Mech. Phys. Solids **105**, 179 (2017).
[21] X. Li, Y. Chen, G. Hu, and G. Huang, A self-adaptive metamaterial beam with digitally controlled resonators for subwavelength broadband flexural wave attenuation, Smart Mater. Struct. **27**, 045015 (2018).
[22] C. Sugino, M. Ruzzene, and A. Erturk, An analytical framework for locally resonant piezoelectric metamaterial plates, Int. J. Solids Struct. **182-183**, 281 (2020).
[23] P. Wang, F. Casadei, S. Shan, J. C. Weaver, and K. Bertoldi, Harnessing Buckling to Design Tunable Locally Resonant Acoustic Metamaterials, Phys. Rev. Lett. **113**, 014301 (2014).
[24] V. Candido de Sousa, C. Sugino, C. De Marqui Junior, and A. Erturk, Adaptive locally resonant metamaterials leveraging shape memory alloys, J. Appl. Phys. **124**, 064505 (2018).
[25] B.-I. Popa, L. Zigoneanu, and S. A. Cummer, Tunable active acoustic metamaterials, Phys. Rev. B **88**, 024303 (2013).
[26] K. Yi, M. Ouisse, E. Sadoulet-Reboul, and G. Matten, Active metamaterials with broadband controllable stiffness for tunable band gaps and non-reciprocal wave propagation, Smart Mater. Struct. **28**, 065025 (2019).
[27] C. Sugino, M. Ruzzene, and A. Erturk, Design and analysis of piezoelectric metamaterial beams with synthetic impedance shunt circuits, IEEE/ASME Trans. Mechatron. **23**, 2144 (2018).
[28] A. J. Fleming, S. Behrens, and S. O. R. Moheimani, Synthetic impedance for implementation of piezoelectric shunt-damping circuits, Electron. Lett. **36**, 1525 (2000).
[29] J. Nečásek, J. Václavík, and P. Marton, in *2017 IEEE International Workshop of Electronics, Control, Measurement, Signals and their Application to Mechatronics (ECMSM)* (IEEE, Donostia-San Sebastian, Spain, 2017), p. 1.
[30] M. I. Hussein and M. J. Frazier, Metadamping: An emergent phenomenon in dissipative metamaterials, J. Sound Vib. **332**, 4767 (2012).
[31] Y. Xia, M. Ruzzene, and A. Erturk, Dramatic bandwidth enhancement in nonlinear metastructures via bistable attachments, Appl. Phys. Lett. **114**, 093501 (2019).
[32] J. Tang and K.-W. Wang, Active-passive hybrid piezoelectric networks for vibration control: Comparisons and improvement, Smart Mater. Struct. **10**, 794 (2001).